International Communications in Heat and Mass Transfer 86 (2017) 117–125

Contents lists available at ScienceDirect

International Communications in Heat and Mass Transfer

journal homepage: www.elsevier.com/locate/ichmt

Critical condition for Rayleigh-Bénard convection of Bingham fluids in rectangular enclosures

O. Turan[a,b], S. Yigit[a], N. Chakraborty[a,*]

[a] School of Mechanical and Systems Engineering, Newcastle University, Claremont Road, Newcastle-Upon-Tyne NE1 7RU, UK
[b] Department of Mechanical Engineering, Bilecik Şeyh Edebali University, Bilecik 11230, Turkey

ARTICLE INFO

Keywords:
Rayleigh-Bénard convection
Yield stress fluids
Constant wall temperature
Constant wall heat flux
Rectangular enclosure

ABSTRACT

Two-dimensional steady-state numerical simulations have been conducted for laminar Rayleigh-Bénard convection of Bingham fluids in rectangular enclosures to analyse the critical Rayleigh number Ra_{crit} for which convection ceases to influence the thermal transport and thermal conduction becomes the principal heat transfer mechanism. The influences of Bingham number Bn on the critical Rayleigh number Ra_{crit} have been investigated for different values of aspect ratio (height: length) AR (ranging from 1/4 to 4) and nominal Prandtl number Pr (ranging from 10 to 500) for both constant wall temperature (CWT) and constant wall heat flux (CWHF) boundary conditions for the horizontal walls. It has been found that Ra_{crit} increases with increasing values of Bn and AR, regardless of the boundary condition. The values of Ra_{crit} have been found to be greater in the case of CWT boundary condition than in the CWHF configuration for $AR \leq 1$, whereas an opposite trend is obtained for $AR > 1$ for Bingham fluids. Additionally, Ra_{crit} has been found be insensitive to the change of Pr for Newtonian fluids (i.e. $Bn = 0$), whereas Ra_{crit} increases with increasing Pr for Bingham fluids irrespective of the boundary condition. A detailed scaling analysis has also been performed to elucidate the effects of Bn,Pr,AR on Ra_{crit} for Bingham fluids. The results of scaling analysis and numerical findings have been utilised to propose a new correlation for Ra_{crit} for both Newtonian and Bingham fluids in the case of both CWT and CWHF boundary conditions.

1. Introduction

Natural convection of yield stress fluids in enclosed spaces plays a pivotal role in many practical applications such as food and chemical processing and nuclear waste cooling etc. Some magneto-rheological and electro-rheological fluids exhibit yield stress behaviour (acts as a solid and does not flow until a threshold yield stress is surpassed), and it is possible to modify the yield stress by applying electrical or magnetic fields [1]. This may be useful for the purpose of controlling heat transport in enclosed spaces (i.e. storage of cryogenics, solar collectors, and nuclear waste cooling). Therefore, several studies have recently been carried out on natural convection of yield stress fluids in enclosed spaces [2–14]. Different configurations for natural convection in enclosed spaces are possible depending on the boundary conditions of the enclosure walls. One of the most important natural convection configurations is the Rayleigh-Bénard convection where the horizontal walls are kept at different temperatures with the bottom wall having the higher temperature. It is well known that the buoyancy force overcomes viscous forces and flow initiates only when the Rayleigh number exceeds a critical value [2] in the Rayleigh-Bénard configuration. Recently, a number of studies focused on the effects of yield stress on the hydrodynamic stability of Rayleigh-Bénard natural convection [3–7]. However, the effects of yield stress on the critical Rayleigh number for laminar Rayleigh-Bénard convection of Bingham fluids in rectangular enclosures are yet to be analysed in detail in existing literature. Thus, the aim of this paper is to investigate the effects of yield stress, Prandtl number and aspect ratio on the critical Rayleigh number in the Rayleigh-Bénard configuration using the Bingham model. In the present study, the influences of Bingham number, aspect ratio and nominal Prandtl number on the critical Rayleigh number for the onset of Rayleigh-Bénard convection have been numerically analysed for different values of aspect ratio (height:length) AR (ranging from 1/4 to 4) and nominal Prandtl number Pr (ranging from 10 to 500) for both constant wall temperature (CWT) and constant wall heat flux (CWHF) boundary conditions for the horizontal walls. The rest of the article will be organised as follows. The necessary mathematical formulation and boundary conditions will be presented in the next section, which will be followed by a detailed scaling analysis. Following this, results will be presented and subsequently discussed. The main findings are summarised and conclusions are drawn in the final section.

* Corresponding author.
E-mail address: nilanjan.chakraborty@ncl.ac.uk (N. Chakraborty).

http://dx.doi.org/10.1016/j.icheatmasstransfer.2017.05.013

Available online 15 June 2017

Nomenclature

AR [−] Aspect ratio
Bn [−] Bingham number
c_p [J/kgK] Specific heat at constant pressure
CWT [−] Constant wall temperature
CWHF [−] Constant wall heat flux
f_1 [−] Function
g [m/s^2] Gravitational acceleration
Gr [−] Grashof number
h [W/m^{2}K] Heat transfer coefficient
H [m] Height of the enclosure
k [W/mK] Thermal conductivity
k_{1-3} [−] Correlation parameters
L [m] Length of the enclosure
Nu [−] Nusselt number
P [Pa] Pressure
Pr [−] Prandtl number
q [W/m^2] Heat flux
Q [W] Heat transfer rate
Ra [−] Rayleigh number
T [K] Temperature
u_i [m/s] ith velocity component
ϑ [m/s] Characteristic velocity
x_i [m] Coordinate in ith direction
α [m^2/s] Thermal diffusivity
β [1/K] Coefficient of thermal expansion
δ [m] Velocity boundary layer thickness
δ_{th} [m] Thermal boundary layer thickness
μ [Ns/m^2] Plastic viscosity
μ_{yield} [Ns/m^2] Yield viscosity
ν [m^2/s] Kinematic viscosity
ρ [kg/m^3] Density
$\dot{\gamma}$ [1/s] Second invariant of strain rate tensor
$\dot{\gamma}_{ij}$ [1/s] Components of strain rate tensor
$\underline{\underline{\dot{\gamma}}}$ [1/s] Strain rate tensor
$\bar{\tau}$ [N/m^2] Second invariant of viscous stress tensor
τ_{ij} [N/m^2] Components of viscous stress tensor
$\underline{\underline{\tau}}$ [N/m^2] Viscous stress tensor
$\bar{\tau}_y$ [N/m^2] Yield stress
ΔT [K] Difference between hot and cold wall temperature

Subscripts

adv Advective
$Bn = 0$ Newtonian fluid
C Cold wall
crit Critical value
diff Diffusive
eff Effective value
H Hot wall
ref Reference value
wall Wall value

2. Mathematical background

2.1. Constitutive equations and non-dimensional numbers

The strain rate dependence of viscous stresses according to the Bingham model [15] is expressed as:

$$\underline{\underline{\dot{\gamma}}} = 0 \text{ for } \tau \le \tau_y \text{ and } \underline{\underline{\tau}} = \left(\mu + \frac{\tau_y}{\dot{\gamma}}\right)\underline{\underline{\dot{\gamma}}} \text{ for } \tau > \tau_y \tag{1}$$

where the components of the rate of strain tensor $\underline{\underline{\dot{\gamma}}}$ are given by: $\dot{\gamma}_{ij} = ((\partial u_i/\partial x_j + \partial u_j/\partial x_i))$, $\underline{\underline{\tau}}$ is the stress tensor, τ_y is the yield stress, μ is the plastic viscosity. In Eq. (1), τ and $\dot{\gamma}$ are the second invariants of the stress and the rate of strain tensors respectively, which are expressed as:

$$\tau = \left[\frac{1}{2}\,\underline{\underline{\tau}}:\underline{\underline{\tau}}\right]^{1/2} \text{ and } \dot{\gamma} = \left[\frac{1}{2}\,\underline{\underline{\dot{\gamma}}}:\underline{\underline{\dot{\gamma}}}\right]^{1/2} \tag{2}$$

Here, the bi-viscosity regularisation [16] is used to model the stress-shear rate characteristics for Bingham fluids:

$$\underline{\underline{\tau}} = \mu_{yield}\,\underline{\underline{\dot{\gamma}}} \text{ for } \dot{\gamma} \le \frac{\tau_y}{\mu_{yield}} \text{ and } \underline{\underline{\tau}} = \tau_y\left(\frac{\underline{\underline{\dot{\gamma}}}}{\dot{\gamma}}\right) + \mu\,\underline{\underline{\dot{\gamma}}} \text{ for } \dot{\gamma} > \tau_y \Big/ \mu_{yield} \tag{3}$$

where μ_{yield} is the yield viscosity. O'Donovan and Tanner [16] demonstrated that a value of $\mu_{yield} \ge 1000\mu$ mimics the true Bingham model in a satisfactory manner. Thus, $\mu_{yield}/\mu = 10^4$ is chosen here for the sake of ensuring high-fidelity of the computational results. The bi-viscosity regularisation (i.e. Eq. (3)) converts the "unyielded" region to a zone of high viscosity such that the numerical solutions predict negligible magnitudes of velocity in these regions. Thus, heat transfer in unyielded regions takes place principally due to conduction.

In the present study, the nominal Rayleigh, Prandtl, and Bingham (i.e. ratio of yield stress to viscous stress) numbers are defined in the following manner for CWT and CWHF boundary conditions:

$$Ra_{CWT} = \frac{\rho g\beta(T_H - T_C)H^3}{\mu\alpha} = Gr_{CWT}Pr \text{ and } Bn_{CWT} = \frac{\tau_y H}{\mu\sqrt{g\beta(T_H - T_C)H}} \tag{4i}$$

$$Ra_{CWHF} = \frac{\rho g\beta q H^4}{k\mu\alpha} = Gr_{CWHF}Pr \text{ and } Bn_{CWHF} = \frac{\tau_y}{\mu\sqrt{g\beta q/k}} \tag{4ii}$$

where $Pr = \mu c_p/k$ is the nominal Prandtl number and $Gr_{CWT} = \rho^2 g\beta(T_H - T_C)H^3/\mu^2$ ($Gr_{CWHF} = \rho^2 g\beta q H^4/k\mu^2$) is the nominal Grashof number for the CWT (CWHF) boundary condition. The local heat transfer coefficient h can be expressed as $h = |-k(\partial T/\partial x_2)_{wf} \times 1/(T_{wall} - T_{ref})|$ where the subscript 'wf' refers to the condition of the fluid in contact with the wall. Here, T_{wall} is the wall temperature and T_{ref} is the appropriate reference temperature, which can be taken to be the temperature of the hot (cold) wall. Accordingly, the mean the heat transfer coefficient $\bar{h}$ and the mean Nusselt number $\overline{Nu}$ can be evaluated as:

$$\bar{h} = \left(\frac{1}{L}\right)\int_0^L h dx_1 \text{ and } \overline{Nu} = \bar{h}H \Big/ k \tag{5}$$

2.2. Governing equations and boundary conditions

The steady-state conservation equations for mass, momentum, and energy for incompressible Bingham fluids take the following form:

$$\frac{\partial u_i}{\partial x_i} = 0 \tag{6}$$

$$\rho u_j\frac{\partial u_i}{\partial x_j} = -\frac{\partial P}{\partial x_i} + \rho g\beta\delta_{i2}(T - T_{ref}) + \frac{\partial \tau_{ij}}{\partial x_j} \tag{7}$$

$$\rho u_j c_p \frac{\partial T}{\partial x_j} = \frac{\partial}{\partial x_j}\left(k\frac{\partial T}{\partial x_j}\right) \tag{8}$$

where the cold wall temperature is taken to be the reference temperature for evaluating the buoyancy term $\rho g\delta_{i2}\beta(T - T_C)$ in the momentum conservation equations following several previous studies [2,9–11,20] for the CWT boundary condition. By contrast, the temperature at the geometric centre of the domain is taken to be T_{ref} in the case of CWHF boundary condition. The Kronecker's delta δ_{i2} ensures that the buoyancy term remains operational only in the momentum equation for the vertical direction (i.e. x_2-direction). The bi-viscosity model [16] (see Eq. (3)) is used to model the viscous effects of the Bingham fluids in Eq. (7). The simulation domain is shown schematically in Fig. 1 where the two horizontal walls of a rectangular enclosure are subjected to either CWT or CWHF boundary condition, whereas the other boundaries are considered to be adiabatic in nature. The velocity components (i.e. $u_1 = 0$ and $u_2 = 0$) are identically zero on each boundary because of the no-slip condition and impenetrability of rigid boundaries. For the CWHF configuration, the heat fluxes for the cold and hot vertical walls are specified (i.e. $-k(\partial T/\partial x_2)|_{x_2} = 0 = q$ and $-k(\partial T/\partial x_2)|_{x_2} = H = q$). In contrast, for the CWT configuration, the temperatures for the hot and cold vertical walls are specified (i.e. $T(x_2 = 0) = T_H$ and $T(x_2 = H) = T_C$). The temperature boundary conditions for the vertical insulated boundaries are given by: $\partial T/\partial x_1 = 0$ at $x_1 = 0$ and $x_1 = L$.

The steady-state conservation equations of mass, momentum, and energy equations are solved in the framework of the finite-volume methodology where a second-order central differencing scheme is used for the diffusive terms and a second-order up-wind scheme is used for the convective terms. The well-known SIMPLE (Semi-Implicit Method for Pressure-Linked Equations) algorithm [17] is used for the coupling of the pressure and velocity and the convergence criteria were set to 10^{-6} for all the relative (scaled) residuals for the iterative solution method. A detailed analysis has been conducted using a number of different non-uniform meshes in order to establish grid independent results for both Newtonian (i.e. $Bn = 0$) and Bingham fluids. The simulation results have been benchmarked with respect to previous findings for Newtonian [18] and Bingham fluids [19]. Interested readers are referred to Ref. [10,20] for detailed information about benchmarking and grid independence studies.

3. Scaling analysis

In the case of natural convection of Bingham fluids, it would have been more appropriate to use an effective viscosity μ_{eff} in the definition of Rayleigh number. An effective Rayleigh number for CWT and CWHF boundary conditions can be defined in the following manner:

$$Ra_{CWT,eff} = \frac{\rho^2 c_p g\beta\Delta T H^3}{\mu_{eff}\, k} \text{ and } Ra_{CWHF,eff} = \frac{\rho^2 c_p g\beta q H^3}{\mu_{eff}\, k^2} \tag{9}$$

where the effective viscosity can be estimated as:

$$\mu_{eff} = \tau_y/\dot{\gamma} + \mu \tag{10}$$

which can be scaled in the following manner in the boundary layer on the horizontal walls:

$$\mu_{eff} \sim \tau_y \delta/u_1 + \mu \tag{11}$$

In order to estimate the hydrodynamic boundary layer thickness δ, the equality of the order of magnitudes of inertial and viscous forces in the horizontal direction (i.e. x_1-direction) is considered:

$$\rho {u_1}^2/L \sim \tau/\delta \tag{12}$$

where u_1 is a characteristic velocity scale. For Bingham fluids the shear stress τ can be estimated as: $\tau \sim \tau_y + \mu u_1/\delta$, which upon substitution in Eq. (12) provides:

$$\rho {u_1}^2/L \sim (\tau_y + \mu u_1/\delta)1/\delta \tag{13}$$

Based on Eq. (13) the hydrodynamic boundary layer thickness can be estimated as:

$$\delta \sim \frac{1}{2}\frac{\tau_y L}{\rho {u_1}^2} + \frac{1}{2}\frac{L}{\rho {u_1}^2}\sqrt{{\tau_y}^2 + 4\rho\frac{{u_1}^3}{L}\mu} \tag{14}$$

For natural convection, the flow is induced by the buoyancy force and thus equating the order of magnitudes of the inertial and buoyancy forces in the boundary layer adjacent to the vertical walls $({u_2}^2/H \sim g\beta\Delta T)$ provides an expression for the characteristic velocity scale in the vertical direction as: $u_2 \sim \sqrt{g\beta\Delta T H}$ $(u_2 \sim \sqrt{g\beta q \delta_{th} H/k})$ for the CWT (CWHF) boundary condition. Upon using continuity that leads to a scaling estimate for the velocity scale in the boundary layer adjacent to the horizontal wall:

$$u_1 \sim \frac{u_2}{AR} \sim \frac{\sqrt{g\beta\Delta T H}}{AR} \text{ for CWT} \tag{15i}$$

$$u_1 \sim \frac{u_2}{AR} \sim \frac{\sqrt{\frac{g\beta q \delta_{th} H}{k}}}{AR} \text{for CWHF} \tag{15ii}$$

Using Eqs. (15i) and (15ii) in Eq. (14) and the definitions of Bn and Pr one obtains the following estimates of the hydrodynamic boundary layer thickness δ:

$$\frac{\delta}{H} \sim \sqrt{Pr/Ra}\left[0.5BnAR + 0.5\sqrt{(BnAR)^2 + 4(Ra/Pr)^{\frac{1}{2}}}\right] \text{for CWT} \tag{16i}$$

$$\sqrt{Ra/Pr} f_1^{-1/2}(\delta/H)^{5/2} \sim (BnAR) f_1^{1/2}(\delta/H)^{1/2} + 1 \text{ for CWHF} \tag{16ii}$$

where $f_1 (= \delta/\delta_{th})$ is a function of Ra, Pr, Bn and AR, which is expected

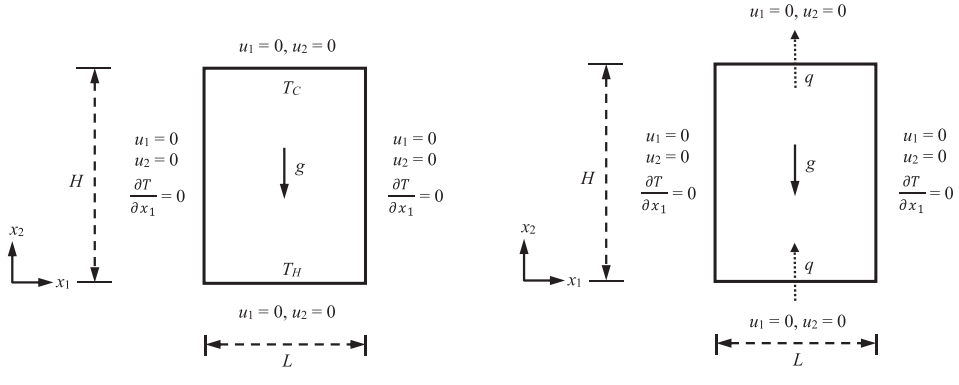

Fig. 1. Schematic diagram of the simulation domain: (a) CWT, (b) CWHF boundary conditions.

to increase with increasing nominal Prandtl number. Using Eqs. (15i), (15ii) and Eqs. (16i) and (16ii) in Eq. (14), μ_{eff} can be estimated based on Eq. (9), which provides an estimation of the effective Rayleigh number as:

$$Ra_{CWT,eff} = Ra\{1 + 0.5BnAR(Pr/Ra)^{1/2}[BnAR + \sqrt{(BnAR)^2 + 4(Ra/Pr)^{1/2}}]\}^{-1} \quad (17i)$$

$$Ra_{CWHF,eff} = Ra\{1 + (BnAR)f_1^{1/2}(\delta/H)^{1/2}\}^{-1} \quad (17ii)$$

This scaling estimates given by Eqs. ((9)–(17i), (17ii)) provide useful insight into the behaviour of Ra_{eff} in response to the variations of Bn, Pr and AR in Rayleigh-Bénard convection of Bingham fluids in rectangular enclosures.

4. Results and discussion

It is worth noting that Bingham fluid flow is unconditionally stable under the quiescent flow initial condition [3], and thus the steady-state solutions for Newtonian (i.e. $Bn = 0$) fluids are used as the initial conditions for Bingham fluid simulations in Rayleigh-Bénard convection configuration. Additionally, the values of Ra_{crit} are evaluated by reducing Ra in steps of 1.0 from an established flow condition until $\overline{Nu}$ reduces to 1.00 (i.e. indicating thermal conduction-driven transport) for

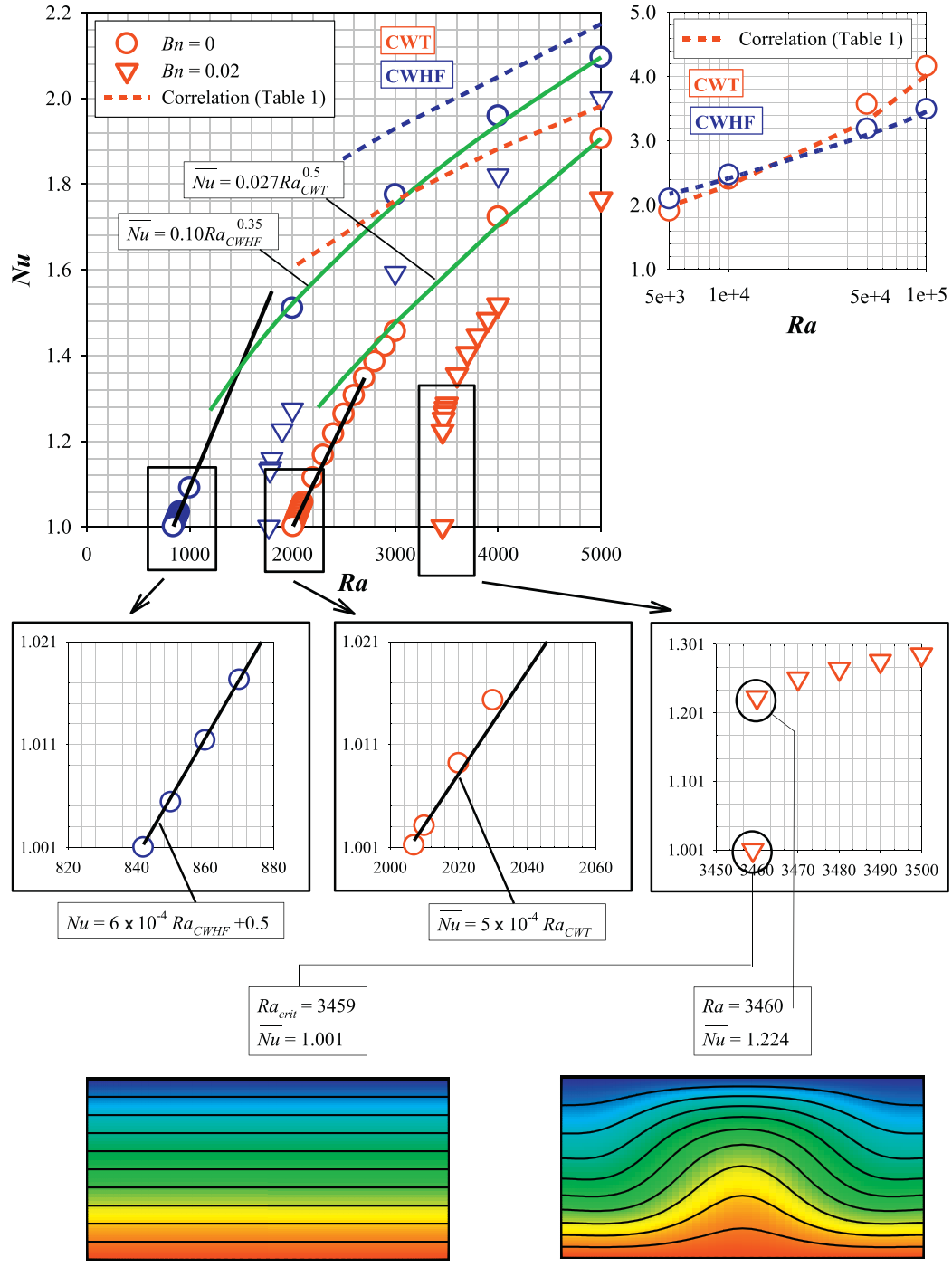

Fig. 2. The variation of $\overline{Nu}$ with Ra for both CWT and CWHF boundary conditions at $Pr = 100$ and $AR = 0.5$ for both Newtonian (i.e.$Bn = 0$) and Bingham (i.e.$Bn = 0.02$) fluids and the temperature isotherms for $Ra_{crit} = 3459$ and $Ra = 3460$ for Bingham (i.e.$Bn = 0.02$) fluid case for CWT boundary condition.

a given set of values of AR, Pr and Bn (see in Fig. 2). The variation of $\overline{Nu}$ with Ra is shown in Fig. 2 for both CWT and CWHF boundary conditions at $Pr = 100$ and $AR = 0.5$ for both Newtonian (i.e. $Bn = 0$) and Bingham (i.e. $Bn = 0.02$) fluids. In the case of Newtonian fluids (i.e. $Bn = 0$), the instability is known to be super-critical since $\overline{Nu}$ decreases gradually with decreasing Ra and eventually settles to 1.00 indicating a purely conduction-driven transport. For $Ra \sim Ra_{crit}$, it is possible to equate the order of magnitudes of the advective and diffusive terms of the energy transport equation to obtain: $q/H \sim \rho c_p u_2 \Delta T/H$, which leads to $h = q/\Delta T \sim k u_2/\alpha$ or $Nu = hH/k \sim \sqrt{g\beta\Delta T H^3/\alpha}$. Thus, the mean Nusselt number $\overline{Nu}$ for Newtonian fluids is expected to scale as: $\overline{Nu} \sim \sqrt{g\beta\Delta T H^3/\alpha} \sim \sqrt{RaPr}$ ($\overline{Nu} \sim \sqrt{g\beta\Delta T H^3/\alpha} \sim \sqrt{RaPr} \times \sqrt{\delta_{th}/H}$) in the case of CWT (CWHF) boundary condition for $Ra \sim Ra_{crit}$. It can be seen from Fig. 2 that $\overline{Nu}$ varies as $Ra^{0.5}$ ($Ra^{0.35}$) for $Ra \sim Ra_{crit}$ (represented by green lines in Fig. 2) in the case of CWT (CWHF) boundary conditions. In the case of $Ra > Ra_{crit}$ but for $Ra \approx Ra_{crit}$ one can further simplify $\overline{Nu} \sim \sqrt{RaPr}$ using $Ra = Ra_{crit} + x$ (where $x = (Ra - Ra_{crit}) \ll Ra_{crit}$), which upon series expansion yields: $\overline{Nu} \sim 0.5[\,Ra_{crit}^{0.5} + Ra/Ra_{crit}^{0.5}]\sqrt{Pr}$. It can be seen from Fig. 2 that $\overline{Nu}$ in Newtonian fluids indeed shows a linear variation (shown by black solid lines in Fig. 2) with Ra close to the critical condition for CWT boundary condition. A similar linear variation is observed for CWHF boundary condition, which can be explained by a series expansion as done for CWT boundary condition. For an established boundary layer transport regime, substituting $Bn = 0$ in Eq. (16i), and using $\overline{Nu} \sim qH/\Delta T k \sim H/\delta_{th}$ lead to: $\overline{Nu} \sim (Ra/Pr)^{0.25} f_1$ for CWT boundary condition, which is consistent with the behaviour shown by the dashed line, which is given by the mean Nusselt number correlation (see Table 1 for its mathematical expression) proposed by Yigit et al. [2,10]. For CWHF boundary condition, δ_{th}/H is expected to be of the order of unity (i.e. $\delta_{th}/H \sim 1$) for $Ra \approx Ra_{crit}$, and thus the mean Nusselt number for Newtonian fluids, shows a linear variation with Ra before showing a power-law in terms of Ra with a positive exponent smaller than unity (i.e. $\overline{Nu} \sim Ra^{0.35}$), as it can be seen in Fig. 2. It is worth noting that the mean Nusselt number scales as $\overline{Nu} \sim \sqrt{RaPr} \times \sqrt{\delta_{th}/H} \sim Ra^{0.35}$ instead of $\overline{Nu} \sim Ra^{0.5}$ for $Ra \sim Ra_{crit}$ in the CWHF case since δ_{th}/H is also dependent on Ra. Putting $Bn = 0$ in Eq. (16ii) reveals that $H/\delta \sim (Ra/Pr)^{0.2}/f_1^{0.2}$ for the boundary layer transport for well-established Rayleigh-Bénard convection (i.e. $Ra \gg Ra_{crit}$), which leads to $\overline{Nu} \sim H/\delta_{th} \sim (Ra/Pr)^{0.2} f_1^{0.8}$, which is consistent with the correlation proposed by Yigit and Chakraborty [10], as summarised in Table 1.

In contrast to the behaviour of Newtonian fluids, the variation of $\overline{Nu}$ with Ra for a representative Bingham fluid case exhibits a rapid drop of $\overline{Nu}$ to 1.0 at $Ra = Ra_{crit}$ in Fig. 2 after a gradual decrease with decreasing Ra, regardless of the boundary condition. At $\overline{Nu} = 1.0$, the fluid flow ceases to influence the thermal transport and the isotherms become parallel to the horizontal walls indicating conduction-dominated thermal transport. Here, the instability is found to be sub-critical for Bingham fluids, since thermal convection ceases abruptly once Rayleigh number becomes smaller than a threshold critical value (i.e. $Ra \approx Ra_{crit}$).

4.1. Effects of Bingham number

The variations of Ra_{crit} with Bn are shown in Fig. 3 for different values of Pr and AR for both CWT and CWHF boundary conditions. It can be seen from Fig. 3 that Ra_{crit} increases with increasing Bn, regardless of the boundary condition. The viscous flow resistance in comparison to buoyancy force strengthens with increasing Bn and as a result higher values of Ra_{crit} are needed to overcome the viscous forces to initiate flow within the enclosure. This statement can be supported by scaling estimations given by Eqs. (17i) and (17ii), which indicate that $Ra_{CWT,eff}$ and $Ra_{CWHF,eff}$ decrease with increasing Bn as a result of the weakening of advective transport. Thus, higher values of Ra in the Bingham fluid cases are needed than the corresponding Newtonian fluid cases in order to have values of Ra_{eff} which allow for convection within the enclosure. Furthermore, the values of Ra_{crit} for Bingham fluids in the case of CWT boundary condition has been found to be greater than those in the CWHF configuration for $AR \leq 1$, whereas an opposite trend has been obtained for $AR > 1$. In order to understand this behaviour it is worth investigating the energy flux integral at the vertical mid-plane for well-established convective transport (i.e. $Ra \gg Ra_{crit}$) [2,10]:

$$Q = Q_{adv} + Q_{diff} = \int_0^H \rho c_p u_1 \Delta T dx_2 - \int_0^H k(\partial T/\partial x_1) dx_2 \tag{18}$$

where:

$$Q_{adv} = \int_0^H \rho c_p u_1 \Delta T dx_2 \approx \int_0^\delta \rho c_p u_1 \Delta T dx_2 \tag{19i}$$

$$Q_{diff} = -\int_0^H k(\partial T/\partial x_1) dx_2 \tag{19ii}$$

Substituting Eqs. ((15i), (15ii)) and ((16i), (16ii)) in Eqs. (19i) and (19ii) respectively yields the following scaling estimates for the maximum magnitudes of Q_{adv} and Q_{diff} for both CWT and CWHF cases:

$$Q_{adv} \sim \rho c_p u_1 \Delta T \delta \sim 0.5(k\Delta T) Pr\,[Bn + \sqrt{Bn^2 + 4(Ra/Pr)^{1/2}/AR^2}\,] \text{ for CWT} \tag{20i}$$

$$Q_{diff} \sim -\int_0^H k\left(\frac{\partial T}{\partial x_1}\right) dx_2 \sim (k\Delta T) AR \text{ for CWT} \tag{20ii}$$

$$Q_{adv} \sim \frac{\rho c_p u_1 q \delta_{th} \delta}{k} \sim qH\sqrt{RaPr}\left(\frac{\delta}{H}\right)^{\frac{5}{2}} AR^{-1} f_1^{-\frac{3}{2}} \text{ for CWHF} \tag{21i}$$

$$Q_{diff} \sim -\int_0^H k\left(\frac{\partial T}{\partial x_1}\right) dx_2 \sim qH\left(\frac{\delta}{H}\right) AR f_1^{-1} \text{ for CWHF} \tag{21ii}$$

It is also worth noting that above scaling estimations are only valid when convection is well-established but useful insights can still be extracted regarding the relative influences of advection and diffusion on overall thermal transport. It is not possible to express Eq. (16ii) analytically, but useful limiting conditions can be inferred from the above scaling relations. For large values of ($Bn\,AR$), Eq. (16ii) becomes: $\delta/H \sim (BnAR)^{1/2}(Pr/Ra)^{1/4} f_1^{1/2}$. This provides an estimation of the maximum magnitude of Q_{diff} in the case of CWHF boundary condition as $Q_{diff} \sim qH(Pr/Ra)^{1/4} Bn^{1/2} AR^{3/2} f_1^{-1}$. This scaling estimation shows that Q_{diff} strengthens with increasing AR and Bn when q, Ra and Pr are held constant for the CWHF configuration. Similarly, Q_{diff} strengthens with increasing AR (see Eq. (20ii)) in the case of CWT boundary condition. By contrast, the contribution of Q_{adv} strengthens with decreasing AR for both boundary conditions. A comparison between $Q_{diff} \sim qH(Pr/Ra)^{1/4} Bn^{1/2} AR^{3/2} f_1^{-1}$ (for CWHF) and $Q_{diff} \sim (k\Delta T) AR$ reveals that the augmentation of diffusive transport with increasing Bn is stronger in the CWHF boundary condition than in the CWT configuration and this trend strengthens (weakens) with increasing AR for $AR > 1$ ($AR < 1$), as can be substantiated from Fig. 3. The above scaling relations also suggest that a greater (smaller) value of Ra_{crit} is needed to overcome the diffusive transport for the CWT configuration

Table 1
Summary of the mean Nusselt number $\overline{Nu}$ correlations for Rayleigh-Bénard convection of Newtonian (i.e. $Bn = 0$) fluids in rectangular enclosures.

$\overline{Nu} = [\{m_0/[1 + exp\{(AR - x_0)/n_0\}]\} - y_0]\,\lvert AR - 1\rvert^{0.01} + \overline{Nu}\,(AR = 1)$	
CWT	$\overline{Nu}\,(AR = 1) = 0.178Ra^{0.269}[Pr/(1 + Pr)]^{0.02}$
	$x_0 = 0.55 + 29.25\exp[-0.5\{(lnRa - 11.12)/0.306\}^2]$
	$y_0 = 0.455 + 4097/[1 + \exp\{(46754 - Ra)/4258\}]$
	$m_0 = 0.765 + 4097/[1 + \exp\{(46743 - Ra)/4270\}]$
	$n_0 = 0.022 + 3.31\exp[-0.5\{(lnRa - 11.10)/0.301\}^2]$
CWHF	$\overline{Nu}\,(AR = 1) = 0.289Ra^{0.214}[Pr/(1 + Pr)]^{0.017}$
	$x_0 = 0.613 + 2.21/[1 + \exp\{(10.43 - lnRa)/0.42\}]$
	$y_0 = -33.6 + 40.95/[1 + \exp\{(-lnRa - 4.658)/8.03\}]$
	$m_0 = 0.767 + 1.917/[1 + \exp\{(9.194 - lnRa)/0.715\}]$
	$n_0 = 0.04 + 0.69/\{1 + [(lnRa - 11)/0.644]^2\}$

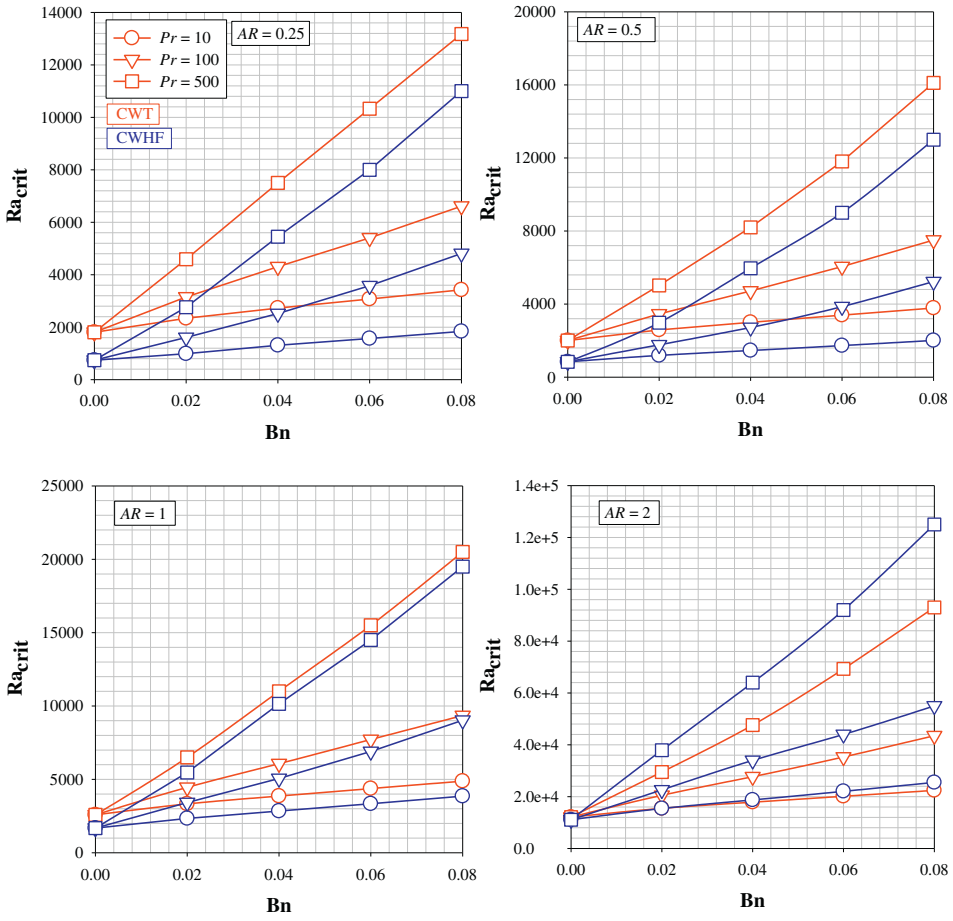

Fig. 3. The variations of Ra_{crit} with Bn for different values of Pr and AR for both CWT and CWHF boundary conditions.

than in the case of CWHF boundary condition for $AR < 1$ ($AR > 1$).

4.2. Effects of Prandtl number

The effects of Pr on Ra_{crit} for both CWT and CWHF boundary conditions are shown in Fig. 4 at different values of Bn and AR for both Newtonian (i.e. $Bn = 0$) and Bingham fluid cases. It is evident from Fig. 4 that Ra_{crit} has been found be independent to the variation of Pr for Newtonian fluids (i.e. $Bn = 0$), whereas Ra_{crit} increases with increasing Pr for Bingham fluids for both CWT and CWHF boundary conditions. Thermal boundary layer is much thinner than the hydrodynamic boundary layer thickness for $Pr \gg 1$ for Newtonian fluids (i.e. $Bn = 0$) and thus a change in Pr modifies the relative balance between the buoyancy and viscous forces, and does not affect the thermal transport within the thermal boundary layer [21]. Therefore, Ra_{crit} remains unaffected by Prandtl number Pr for Newtonian fluids. On the other hand, for Bingham fluids, the scaling predictions for Ra_{eff} given by Eqs. (17i) and (17ii) (note that f_1 is expected to increase with increasing Pr) indicate that both $Ra_{CWT,eff}$ and $Ra_{CWHF,eff}$ decrease with increasing Pr for a given set of values of Bn and AR. This is an evidence of that the relative strength of buoyancy force in comparison to viscous force weakens with increasing Pr. Accordingly, this weakening of buoyancy force with respect to viscous force leads to an increase in Ra_{crit} with increasing Pr for Bingham fluids for both CWT and CWHF boundary conditions.

4.3. Effects of aspect ratio

The influence of AR on Ra_{crit} has been shown in Fig. 5 for both Newtonian (i.e. $Bn = 0$) and Bingham fluid cases for both CWT and CWHF configurations. It can be seen from Fig. 5 that Ra_{crit} increases with increasing AR for both Newtonian (i.e. $Bn = 0$) and Bingham fluids, regardless of the boundary condition. This can be seen as an indicator of weakening of advective transport with increasing AR. This can be explained by the scaling estimations of Q_{adv} and Q_{diff} given by Eqs. ((20i), (20ii)) and ((21i), (21ii)). Eqs. ((20i), (20ii)) and ((21i), (21ii)) indicate that Q_{adv} (Q_{diff}) weakens (strengthens) with increasing AR for both Newtonian and Bingham fluids in the case of both CWT and CWHF boundary conditions. For this reason, the value of Ra_{crit} increases with increasing AR for both Newtonian and Bingham fluids (see Fig. 5), regardless of the boundary condition. The observation for Bingham fluids in Fig. 5 can further be explained by the scaling estimation of Ra_{eff} (i.e. Eqs. (17i), (17ii)). It is expected from Eqs. (17i) and (17ii) that $Ra_{CWT,eff}$ and $Ra_{CWHF,eff}$ decrease with increasing AR, which indicates that the advective transport weakens with increasing AR. Therefore, the convection starts to play a significant role in the overall thermal transport at a greater value of Ra_{crit} for higher AR for both CWT and CWHF configurations.

4.4. Parameterisation of the critical Rayleigh number

The value of effective Rayleigh number for the critical Rayleigh number Ra_{crit} can be scaled using Eq. (17i) as:

$$Ra_{eff} \sim \frac{Ra_{crit}}{\{1 + 0.5BnAR(Pr/Ra_{crit})^{1/2}[BnAR + \sqrt{(BnAR)^2 + 4(Ra_{crit}/Pr)^{1/2}}]\}} \quad (22)$$

It is worth noting that Eq. (17ii) indicates that an exact analytical solution does not exist for CWHF configuration. However, the qualitative trend is expected to be the same for both CWT and CWHF boundary conditions, thus, Eq. (22) can be used Ra_{crit} scaling for both CWT and CWHF boundary conditions. Eq. (22) can be rewritten in the following

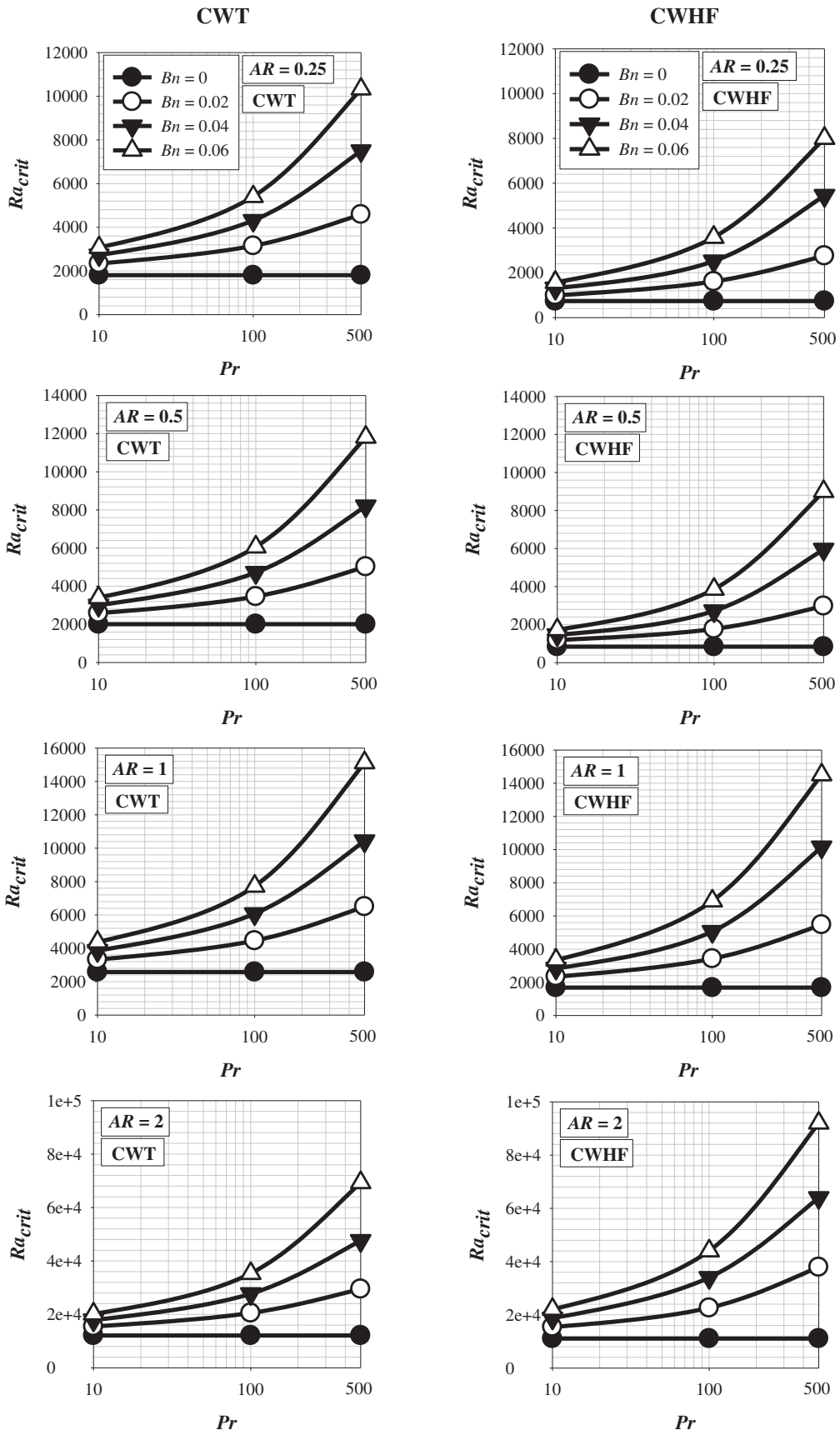

Fig. 4. The variation Ra_{crit} with Pr at different values of Bn and AR for both CWT and CWHF boundary conditions.

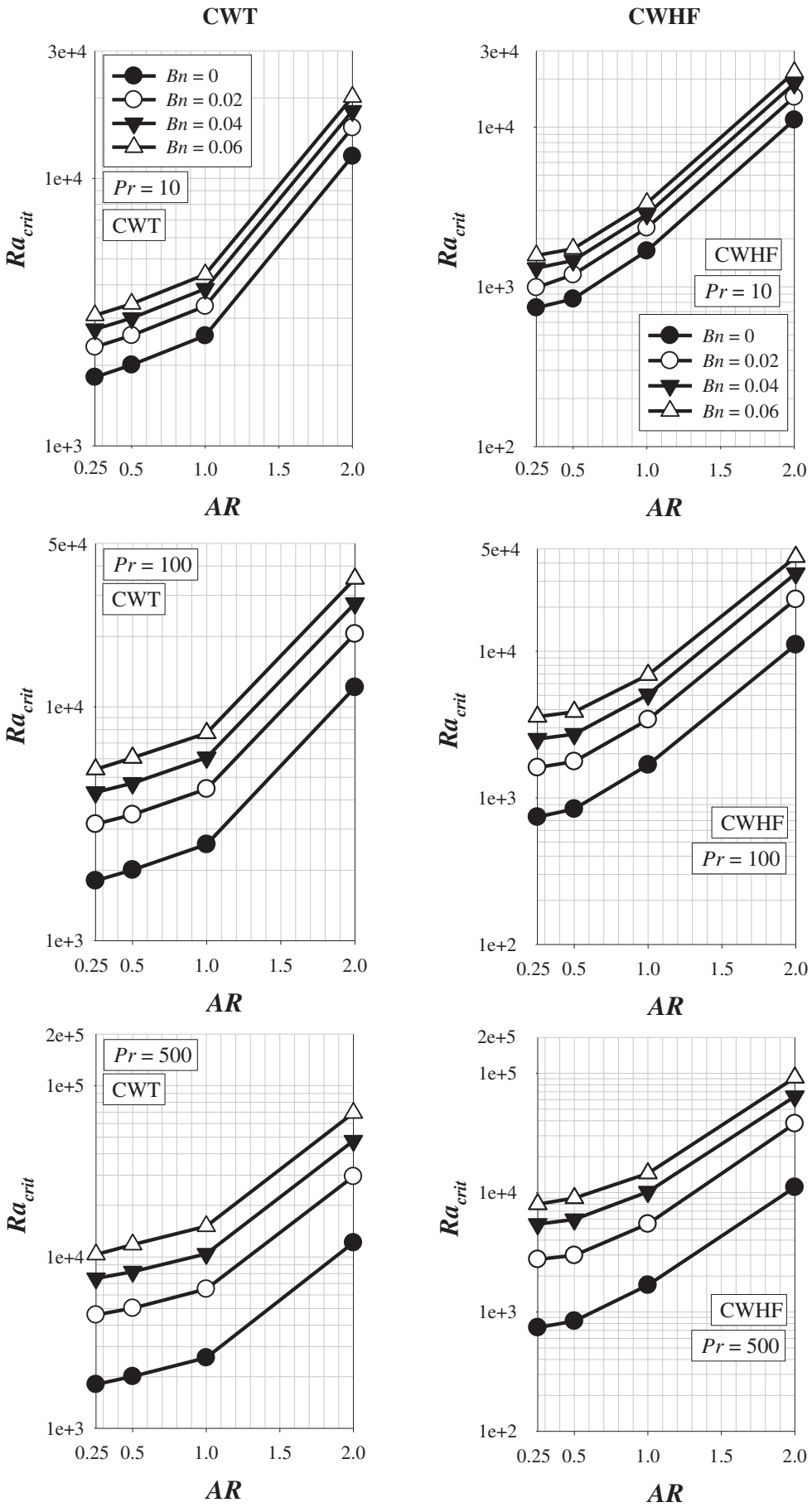

Fig. 5. The variation Ra_{crit} with AR at different values of Bn and Pr for both CWT and CWHF boundary conditions.

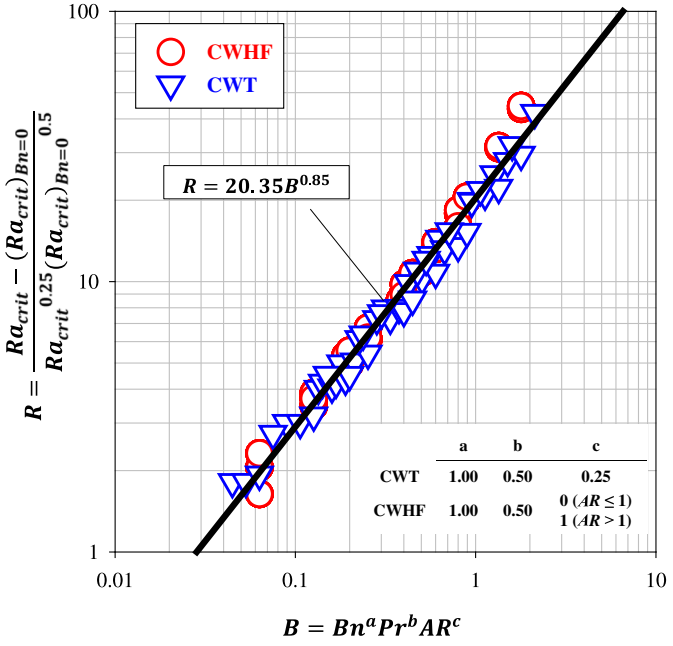

Fig. 6. The variation of $R = (Ra_{crit} - (Ra_{crit})_{Bn=0})/(Ra_{crit}{}^{0.25}(Ra_{crit})_{Bn=0}{}^{0.5})$ with $B = Bn^a Pr^b AR^c$ for different values of Bn, Pr and AR on log-log plot for both CWT and CWHF boundary conditions.

manner:

$$[(Ra_{crit}/Ra_{eff}) - 1] \sim \{0.5 BnAR (Pr/Ra_{crit})^{1/2} [BnAR + \sqrt{(BnAR)^2 + 4(Ra_{crit}/Pr)^{1/2}}]\} \quad (23)$$

Obtaining an expression for $[(Ra_{crit}/Ra_{eff}) - 1](Ra_{crit}/\mathrm{Pr})^{0.5}(2/BnAR)$ from Eq. (23) and squaring it leads to:

$$\left[\frac{(Ra_{crit} - Ra_{eff})}{(Ra_{eff})^{1/2}(Ra_{crit})^{1/4}}\right] \sim BnARPr^{1/4} \quad (24)$$

Eq. (24) can be recast in the following manner:

$$\left[\frac{(Ra_{crit} - (Ra_{crit})_{Bn=0})}{((Ra_{crit})_{Bn=0})^{1/2}(Ra_{crit})^{1/4}}\right] \sim BnARPr^{1/4} \frac{Ra_{eff}{}^{1/2}}{(Ra_{crit})_{Bn=0}{}^{1/2}} + \frac{Ra_{eff} - (Ra_{crit})_{Bn=0}}{(Ra_{crit})_{Bn=0}{}^{1/2}(Ra_{crit})^{1/4}} \quad (25)$$

In Eq. (25), $(Ra_{eff} - (Ra_{crit})_{Bn=0})/(Ra_{crit})_{Bn=0}{}^{1/2}(Ra_{crit})^{1/4}$ can be neglected because, the numerator (i.e. $Ra_{eff} - (Ra_{crit})_{Bn=0}$) is expected to be much smaller in comparison to the denominator (i.e. $(Ra_{crit})_{Bn=0}{}^{1/2}(Ra_{crit})^{1/4}$) of this term. Thus, Eq. (25) can be simplified in the following manner:

$$\left[\frac{(Ra_{crit} - (Ra_{crit})_{Bn=0})}{((Ra_{crit})_{Bn=0})^{1/2}(Ra_{crit})^{1/4}}\right] \sim BnARPr^{1/4} \frac{Ra_{eff}{}^{1/2}}{(Ra_{crit})_{Bn=0}{}^{1/2}} \sim Bn^a AR^b Pr^c \quad (26)$$

The quantity $Ra_{eff}{}^{1/2}/(Ra_{crit})_{Bn=0}{}^{1/2}$ is expected to be dependent on Bn, AR and Pr and thus the right hand side of Eq. (26) can be taken to scale with $Bn^a AR^b Pr^c$. Here, $(Ra_{crit})_{Bn=0}$ correlation proposed for both CWT and CWHF configurations as $(Ra_{crit})_{Bn=0} = k_1 AR^{k_2} + k_3$ where $k_1 = 718$, $k_2 = 3.83$, $k_3 = 1874$ for CWT boundary condition, and $k_1 = 940$, $k_2 = 3.6$, $k_3 = 740$ for CWHF configuration. Finally, correlations have been proposed for the coefficients of a, b and c in Eq. (26). Fig. 6 shows that the variation of $R = (Ra_{crit} - (Ra_{crit})_{Bn=0})/(Ra_{crit}{}^{0.25}(Ra_{crit})_{Bn=0}{}^{0.5})$ with $B = Bn^a Pr^b AR^c$ can be approximated by $R = 20.35B^{0.85}$ for the range of Bn, Pr and AR considered in this analysis. It can be seen from Fig. 6 that a satisfactory level of collapse has been obtained for all Bn, Pr and AR values considered here for both CWT and CWHF boundary conditions. Moreover, the collapse of data in Fig. 6 suggests that numerical/experimental data for Ra_{crit} in the case of Bingham fluids for a combination of Bn, AR and Pr in either of the boundary conditions will be sufficient to predict Ra_{crit} (i.e. approximately 7% avarage uncertainty) for the range Bn, AR and Pr values and boundary conditions considered in this analysis.

5. Conclusions

The influences of Bingham number Bn, aspect ratio AR and nominal Prandtl number Pr on the critical Rayleigh number Ra_{crit} for the onset of Rayleigh-Bénard convection have been numerically analysed. It has been found that Ra_{crit} increases with increasing values of Bn and AR for both CWT and CWHF boundary conditions in case of both Newtonian (i.e. $Bn = 0$) and Bingham fluids. Additionally, Ra_{crit} has been found be insensitive to the change of Pr for Newtonian fluids (i.e. $Bn = 0$), whereas Ra_{crit} increases with increasing Pr for Bingham fluids. It has also been observed that the values of Ra_{crit} in the case of CWT boundary condition are greater than that in the CWHF configuration for $AR \leq 1$. However, an opposite trend has been observed for $AR > 1$. Finally, based on a detailed scaling analysis, a correlation for Ra_{crit} has been purposed for Rayleigh-Bénard convection of Bingham fluids for both CWT and CWHF boundary conditions, which allows for a collapse of the critical Rayleigh number values for Bingham fluids in terms of a combination of Bn, AR and Pr.

Acknowledgements

The authors are grateful to Prof. R. J. Poole of the University of Liverpool for many insightful discussions and Mr. Jake Liver of the Newcastle University for his contribution.

References

[1] N.M. Wereley, Magnetorheology: Advances and Applications, Royal Society of Chemistry, RSC Smart materials, Cambridge, UK, 2014.
[2] S. Yigit, R.J. Poole, N. Chakraborty, Effects of aspect ratio on natural convection of Bingham fluids in rectangular enclosures with differentially heated horizontal walls heated from below, Int. J. Heat Mass Transf. 80 (2015) 727–736.
[3] J. Zhang, D. Vola, I.A. Frigaard, Yield stress effects on Rayleigh-Bénard convection, J. Fluid Mech. 566 (2006) 389–419.
[4] N.J. Balmforth, A.C. Rust, Weakly nonlinear viscoplastic convection, J. Non-Newtonian Fluid Mech. 158 (2009) 36–45.
[5] A. Vikhansky, On the onset of Bingham liquid in rectangular enclosures, J. Non-Newtonian Fluid Mech. 165 (2010) 1713–1716.
[6] Z. Kebiche, C. Castelain, T. Burghelea, Experimental investigation of the Rayleigh-Bénard convection in a yield stress fluid, J. Non-Newtonian Fluid Mech. 203 (2014) 9–23.
[7] M. Darbouli, C. Métivier, J.M. Piau, A. Magnin, A. Abdelali, Rayleigh-Bénard convection for viscoplastic fluids, Phys. Fluids 25 (2013) 023101–023115.
[8] A. Vikhansky, Thermal convection of a viscoplastic liquid with high Rayleigh and Bingham numbers, Phys. Fluids 21 (2009) 103103–103107.
[9] O. Turan, R.J. Poole, N. Chakraborty, Boundary condition effects on natural convection of Bingham fluids in a square enclosure with differentially heated horizontal walls, J. Comput. Therm. Sci. 4 (2012) 77–97.
[10] S. Yigit, N. Chakraborty, Influences of aspect ratio and wall boundary condition on laminar Rayleigh-Bénard convection in rectangular enclosures, Int. J. Numer. Methods Heat Fluid Flow 27 (2017) 310–333.
[11] S. Yigit, S. Chen, P. Quinn, N. Chakraborty, Numerical investigation of laminar Rayleigh-Bénard convection of Bingham fluids in square cross-sectioned cylindrical enclosures, Int. J. Therm. Sci. 110 (2016) 356–368.
[12] M.A. Hassan, M. Pathak, M.K. Khan, Natural convection of viscoplastic fluids in a square enclosure, J. Heat Transf. Trans. ASME 135 (2013) 122501–122512.
[13] M.A. Hassan, M. Pathak, M.K. Khan, Rayleigh-Bénard convection in Herschlel-Bulkley fluid, J. Non-Newtonian Fluid Mech. 226 (2015) 32–45.
[14] D.A.S. Rees, The convection of a Bingham fluid in a differentially-heated porous cavity, Int. J. Numer. Methods Heat Fluid Flow 26 (2016) 879–896.
[15] H.A. Barnes, The yield stress—a review or '$\pi\alpha\nu\tau\alpha\ \rho\varepsilon\iota$'—everything flows? J. Non-Newtonian Fluid Mech. 81 (1999) 133–178.
[16] E.J. O'Donovan, R.I. Tanner, Numerical study of the Bingham squeeze film problem, J. Non-Newtonian Fluid Mech. 15 (1984) 75–83.
[17] S.V. Patankar, Numerical Heat Transfer and Fluid Flow, Hemisphere, Washington, D.C., 1980.
[18] N. Quertatani, N.B. Cheikh, B.B. Beya, T. Lili, Numerical simulation of two dimensional Rayleigh-Bénard convection in an enclosure, C.R. Mec. 336 (2008) 464–470.
[19] D. Vola, L. Boscardin, J.C. Latché, Laminar unsteady flows of Bingham fluids: a numerical strategy and some benchmark results, J. Comput. Phys. 187 (2003) 441–456.
[20] O. Turan, A. Sachdeva, R.J. Poole, N. Chakraborty, Laminar Rayleigh-Bénard convection of yield stress fluids in a square enclosure, J. Non-Newtonian Fluid Mech. 172 (2012) 83–96.
[21] A. Bejan, Convection Heat Transfer, John Wiley Sons Inc., New York, 1984.